J. Fluid Mech. (2011), *vol.* 685, *pp.* 165–190.
doi:10.1017/jfm.2011.296

The intense vorticity structures near the turbulent/non-turbulent interface in a jet

Carlos B. da Silva†, Ricardo J. N. dos Reis and José C. F. Pereira

IDMEC/IST, Technical University of Lisbon, Pav. Mecânica I, 1° andar/esq./LASEF, Av. Rovisco Pais, 1049-001 Lisboa, Portugal

(Received 1 September 2010; revised 28 June 2011; accepted 4 July 2011; first published online 5 September 2011)

The characteristics of the intense vorticity structures (IVSs) near the turbulent/non-turbulent (T/NT) interface separating the turbulent and the irrotational flow regions are analysed using a direct numerical simulation (DNS) of a turbulent plane jet. The T/NT interface is defined by the radius of the large vorticity structures (LVSs) bordering the jet edge, while the IVSs arise only at a depth of about 5η from the T/NT interface, where η is the Kolmogorov micro-scale. Deep inside the jet shear layer the characteristics of the IVSs are similar to the IVSs found in many other flows: the mean radius, tangential velocity and circulation Reynolds number are $R/\eta \approx 4.6$, $u_0/u' \approx 0.8$, and $Re_\Gamma/Re_\lambda^{1/2} \approx 28$, where u_0, and Re_λ are the root mean square of the velocity fluctuations and the Reynolds number based on the Taylor micro-scale, respectively. Moreover, as in forced isotropic turbulence the IVSs inside the jet are well described by the Burgers vortex model, where the vortex core radius is stable due to a balance between the competing effects of axial vorticity production and viscous diffusion. Statistics conditioned on the distance from the T/NT interface are used to analyse the effect of the T/NT interface on the geometry and dynamics of the IVSs and show that the mean radius R, tangential velocity u_0 and circulation Γ of the IVSs increase as the T/NT interface is approached, while the vorticity norm $|\omega|$ stays approximately constant. Specifically R, u_0 and Γ exhibit maxima at a distance of roughly one Taylor micro-scale from the T/NT interface, before decreasing as the T/NT is approached. Analysis of the dynamics of the IVS shows that this is caused by a sharp decrease in the axial stretching rate acting on the axis of the IVSs near the jet edge. Unlike the IVSs deep inside the shear layer, there is a small predominance of vortex diffusion over stretching for the IVSs near the T/NT interface implying that the core of these structures is not stable i.e. it will tend to grow in time. Nevertheless the Burgers vortex model can still be considered to be a good representation for the IVSs near the jet edge, although it is not as accurate as for the IVSs deep inside the jet shear layer, since the observed magnitude of this imbalance is relatively small.

Key words: free shear layers, turbulence simulation, turbulence theory

1. Introduction

The characteristics and dynamics of the vortical structures in turbulent flows is a longstanding issue in turbulence research and has generated a massive amount of

† Email address for correspondence: Carlos.Silva@ist.utl.pt

information over the last 30 yr. Vortical structures consist in regions of concentrated vorticity and low local pressure, with a large lifetime compared with the characteristic time scales of the flow Dubief & Delcayre (2000). The study of these structures is largely motivated by their simplicity and to the possibility of understanding complex flow phenomena using relatively simple models e.g. see Lesieur (1997). Moreover, vortical structures govern the transport, mixing and diffusion of mass, momentum and scalars (e.g. heat) which is important in many applications e.g. understanding the dynamics of the vortical structures is a prerequisite for turbulence control.

It is important to divide the vortical structures present in turbulent flows into two classes: large vorticity structures (LVSs) and intense vorticity structures (IVSs). The LVSs are the largest vortical structures which are present in a particular flow. Often originating in the particular instabilities from that flow, their characteristics such as the vortex core radius, length size and lifetime are deeply related to these processes and therefore are quite different from flow to flow. However the dynamics of these structures share some common features with LVSs from other turbulent flows, e.g. they consist of structures with roughly tubular shape and are approximately governed by the same simple inviscid laws.

On the other hand the IVSs are defined as structures with particularly strong vorticity, i.e. structures composed of flow points with vorticity greater than a particularly high vorticity threshold ω_{ivs}. Jiménez *et al.* (1993) defined this vorticity threshold as equal to the vorticity defining the 1 % of flow points with the highest vorticity. In isotropic turbulence the IVSs are the well-known 'worms' described by Siggia (1981). Many works have been devoted to the study of these structures, particularly in isotropic turbulence e.g. Siggia (1981), Ashust *et al.* (1987), Vincent & Meneguzzi (1991), Jiménez *et al.* (1993) and Jiménez & Wray (1998), but recently other flows have been used to study the IVSs such as mixing layers (Tanahashi, Iwase & Miyauchi 2001), channel flows (Kang, Tanahashi & Miyauchi 2008) and jets (Ganapathisubramani, Lakshminarasimhan & Clemens 2008). In contrast to the LVSs the characteristics of the IVSs are similar in a variety of different flows, e.g. the vortex radius, axial vorticity and azimuthal velocity from the IVSs in mixing layers are similar to the values found in isotropic turbulence. Specifically, it has been reported that the radius of the IVSs is $R \approx 5\eta$, where η is the Kolmogorov micro-scale, in isotropic turbulence (Jiménez *et al.* 1993), mixing layers (Tanahashi *et al.* 2001), channel flows (Kang *et al.* 2008) and jets (Ganapathisubramani *et al.* 2008). That the threshold used to define the IVSs has a negligible impact on their computed characteristics is attested by the fact that other works use different techniques to define the 'worms' obtaining very similar statistics, e.g. Kang *et al.* (2008). In isotropic turbulence Jiménez *et al.* (1993) and Jiménez & Wray (1998) divided the flow structures into three classes: (i) IVSs; (ii) structures of background vorticity, defined as structures with vorticity greater than the fluctuating vorticity and smaller than the vorticity defining the IVSs, i.e. $\omega' < \omega < \omega_{ivs}$; and (iii) weak vorticity structures, with $\omega < \omega'$. It is important to realize that with the notation used here the LVSs are all of the flow vortices that are not included in the set of IVSs, i.e. the LVSs contain also the background vorticity structures and the weak vorticity structures which in isotropic turbulence are relatively free from vorticity and can be identified with the velocity eddies.

The present work focuses on the study of the IVSs in the context of the turbulent entrainment mechanism that takes place in free shear flows such as mixing layers, wakes and jets. In these flows the flow field can be divided into two regions: in one region the flow is turbulent while in the other region the flow consists of largely

irrotational, or non-turbulent flow Corrsin & Kistler (1955). The two regions are separated by a sharp interface, the turbulent/non-turbulent (T/NT) interface, where the turbulent entrainment mechanism takes place. Turbulent entrainment governs the growth rate of free shear layers and also the scalar (e.g. heat) exchanges and the mixing rates across the T/NT interface.

The important role played by the LVSs in the turbulent entrainment has been recognized a long time ago (Townsend 1976). Past studies assumed that turbulent entrainment is mainly caused by large-scale 'engulfing' motions (Townsend 1976) induced by the LVSs. Bisset, Hunt & Rogers (2002) described the topology of the streamlines induced by LVSs near the T/NT interface, and observed that streams of turbulent and irrotational motion collide at the interface, and stretch out along it, driving its highly convoluted shape. The vortical interactions with a T/NT interface were also studied in detail using linear analytical models, e.g. Hunt, Eames & Westerweel (2008).

Recently, some aspects of the LVSs and IVSs near the T/NT interface were investigated by da Silva & Taveira (2010) and da Silva & dos Reis (2011). Specifically, it has been shown that in a jet the T/NT interface is the physical surface defined by the LVSs, in agreement with the classical picture that is known for some time, e.g. Townsend (1966) and Bisset *et al.* (2002): the LVSs are responsible for the observed convolutions of the T/NT interface and explains that the length scale of these convolutions is roughly equal to the length scale of the LVSs. da Silva & dos Reis (2011) showed moreover that the presence of LVSs is responsible for the existence of a region of irrotational kinetic energy dissipation and by a positive enstrophy diffusion in the region bounding the turbulent and the non-turbulent flow regions. The analysis of the orientation of the vortices shows also that the IVSs tend to be aligned with the tangent to the T/NT interface near the jet edge.

The flow vortices also determine the thickness of the T/NT interface, δ_ω. Indeed da Silva & Taveira (2010) have shown that δ_ω in a jet is roughly equal to the radius of the LVSs near the T/NT interface $\delta_\omega \approx R_{lvs}$. The radius of the LVSs near the T/NT interface can be estimated bearing in mind that long-lived vortices are vortices where the time scale associated with the radial viscous diffusion of vorticity is roughly balanced by the axial stretching caused by the local strain rate field S', such as in a Burgers vortex (Jiménez & Wray 1998). The radius of these vortices, even if they are not exactly described by the Burgers vortex model, is at least of the order of the Burgers radius $R_{lvs} \sim (\nu/S')^{1/2}$. In a jet the magnitude of the strain rate acting on a LVS near the jet edge is $S \sim u'/L_{11}$, where u' is the fluctuating velocity field and L_{11} is the integral scale of turbulence (Hunt *et al.* 2010). This leads to $R_{lvs} \sim \sqrt{\nu/(u'/L_{11})} = L_{11}Re_0^{-1/2} \sim \lambda$, where $Re_0 = u'L_{11}/\nu$ is the Reynolds number associated with the integral scale. However, it is possible to find jets (particularly at very high Reynolds numbers) and in shear-free flows (flows without mean shear) where the biggest existing vorticity structures are similar to the IVSs in that they exhibit no particular spatial orientation, due to the fragmentation of the LVSs. In this case $S' \sim u'/\lambda$ and the radius of the vortices defining the T/NT interface is $R_{ivs} \sim \sqrt{\nu/(u'/\lambda)} = \lambda Re_\lambda^{-1/2} \sim \eta$, where $Re_\lambda = u'\lambda/\nu$ is the Reynolds number based on the Taylor micro-scale.

Concerning the physical processes responsible by the entrainment, recent works suggest that the entrainment is mainly caused by small-scale ('nibbling') eddy motions acting on the T/NT interface (Westerweel *et al.* 2005), as proposed originally by Corrsin & Kistler (1955). Specifically Westerweel *et al.* (2005, 2009) showed that the

engulfment motion caused by the large-scale vortices is not the dominant process for the turbulent entrainment of irrotational fluid in a jet, in agreement with Mathew & Basu (2002). Instead, it is suggested that small-scale 'nibbling' eddy motions may be the dominating entrainment mechanism. Nevertheless, it is largely accepted that the *entrainment rate* is imposed by the LVSs that exist inside the turbulent region in the proximity of the T/NT interface. One has to bear in mind that both engulfing and nibbling exist in free shear flows, and that the relative importance between the two processes may depend on the geometry of the flow due to the well-known sensitivity of shear flows to large-scale external initial and boundary conditions or Reynolds number, e.g. Westerweel *et al.* (2009) argue that engulfing may be more important in mixing layers than in jets or wakes.

Whatever these nibbling eddy motions may consist of, they are likely to be more associated with small-scale IVSs than with the LVSs. Notwithstanding the amount of work carried out on the role of the LVSs near the T/NT interface in free shear flows, there is virtually no work devoted to the effects and dynamics of the IVSs in this region. Specifically the dynamics of the IVSs near the T/NT interface remains largely unexplored.

The goal of the present work is to characterize the geometry of the IVSs near the T/NT interface in order to shed light on their dynamics in the context of turbulent entrainment. For this purpose a direct numerical simulation (DNS) of a temporally evolving turbulent plane jet was used. The turbulent plane jet shares many common features with other free shear flows such as the presence of important turbulent diffusion mechanisms driving the growth of the shear layer, and the presence of similar LVSs, such as the Kelvin–Helmholtz vortices originated during the transition to turbulence phase, whose foot prints are still present in the fully developed self-similar turbulent regime.

This article is organized as follows. In § 2 we describe the temporal turbulent plane jet DNS used in the present work. Section 3 analyses the global features of the IVSs in a jet while § 4 studies these characteristics in the proximity of the T/NT interface. The work ends with a review of the main results and conclusions (§ 5).

2. Direct numerical simulation of a turbulent plane jet

In the present work the intense vorticity structures are analysed near the T/NT interface by using a temporal DNS of a turbulent plane jet, which we refer to as P. Jet. This DNS is the same as already used by the authors and described in detail in da Silva & Pereira (2008), da Silva (2009) and da Silva & Taveira (2010).

It is noteworthy that the present simulation is mathematically identical to the plane wake used in Bisset *et al.* (2002), since temporally evolving wakes and planar jets differ mainly in the shape of the initial mean velocity profile: the maximum mean velocity in a jet is located at the centreline while in a wake the minimum velocity is located at the centreline. Consequently in the self-similar regime the shape and magnitude of the Reynolds stresses profiles in the two flows are similar as can be attested by comparing the Reynolds stresses in da Silva & Pereira (2008) and Bisset *et al.* (2002).

The Navier–Stokes solver uses a pseudo-spectral scheme for spatial discretization, and a third-order, three-step, Runge–Kutta scheme for temporal advancement. The grid is isotropic ($\Delta x = \Delta y = \Delta z$), and the number of collocation points along the streamwise (x), normal (y) and spanwise (z) directions is equal to ($N_x \times N_y \times N_z =$

$(256 \times 384 \times 256)$. The extent of the computational domain attains $(L_x, L_y, L_z) = (4H, 6H, 4H)$, where H is the initial jet slot width.

The initial condition consists of a mean velocity profile on which a three-component velocity fluctuating 'spectral noise' was superimposed. Specifically, the mean velocity profile is given by

$$u(x, y, z) = \frac{U_1}{2}\left\{1 + \tanh\left[\frac{H}{4\theta_0}\left(1 - \frac{2|y|}{H}\right)\right]\right\}, \tag{2.1}$$

where U_1 is the mean velocity at the jet centreline and θ_0 is the initial momentum thickness. The non-dimensional ratio between the inlet slot width and the initial momentum thickness was set to $H/\theta_0 = 35$. Similar mean velocity profiles were used in many other simulations of planar jets, e.g. Stanley, Sarkar & Mellado (2002).

The simulations are halted before the effect of the boundary conditions can be observed in the jet statistics, e.g. the Reynolds stresses. Extensive validation tests were undertaken for this simulation and the results showed that the present DNS is accurate at the large and small scales of motion and representative of a fully developed turbulent plane jet (see da Silva & Pereira 2008 for details). The self-similar regime occurs when the second-order moments at several different times collapse, and is obtained at $T/T_{ref} \approx 20$, where $T_{ref} = H/(2U_1)$ by which time the jet half-width is equal to $\delta_{0.5}/H = 0.78$. At the self-similar regime the Reynolds number based on the Taylor micro-scale $\lambda^2 = \langle u'^2\rangle/\langle(\partial u/\partial x)'^2\rangle$, and on the root mean square of the streamwise velocity $u' = \langle u'^2\rangle^{1/2}$ is equal to $Re_\lambda = u'\lambda/\nu \approx 120$ across the jet shear layer. The minimum resolution across the jet shear layer is $\Delta x = \eta \approx 3$ i.e. most points/instants have $\Delta x = \eta < 3$. This is slightly less than in isotropic turbulence but is well in line with the resolution used in the DNS of free shear flows. The kinetic energy and enstrophy spectra shown in da Silva & Pereira (2008) confirm that the resolution is adequate.

The flow coherent structures from the P. Jet DNS are qualitatively similar to many previous DNSs of turbulent plane jets, e.g. Stanley *et al.* (2002). Figure 1(*a*,*b*) show iso-surfaces of $Q > 0$ and pressure, respectively, at the far field (self-similar) regime, where $Q = \omega_i\omega_i/4 + S_{ij}S_{ij}/2$, where $S_{ij} = 1/2(\partial u_i/\partial x_j + \partial u_j/\partial x_i)$ is the rate-of-strain tensor, and ω_i is the vorticity vector. The low-pressure iso-surfaces highlight the big rollers which are remnants of the Kelvin–Helmholtz vortices generated during the transition to turbulence which represent the typical LVSs from a turbulent plane jet. The iso-surfaces of $Q > 0$ highlight smaller, more intense structures, with fewer signs of a particular spatial orientation, except for the streamwise vortices near the jet edges. As expected the IVSs are closer to the structures defined by $Q > 0$ than to the structures defined by regions of low pressure (see below), but there is of course some spatial overlap between these structures.

The present work uses a vortex tracking procedure to detect and characterize the IVSs. In order to validate this vortex tracking procedure a small DNS of (forced) isotropic turbulence was also carried out. We denote this simulation by HIT. This simulation was made using a standard pseudo-spectral code with low wavenumber forcing described in da Silva & Pereira (2007*a*). The simulation uses 256^3 collocation points and the Reynolds number based on the Taylor micro-scale is $Re_\lambda = 111$ and the maximum resolved wavenumber multiplied by the Kolmogorov micro-scale is $k_{max}\eta = 1.51$.

A first comparison of the flow structures present in the two simulations, HIT and P. Jet, can be made using histograms representing the fraction of vorticity and

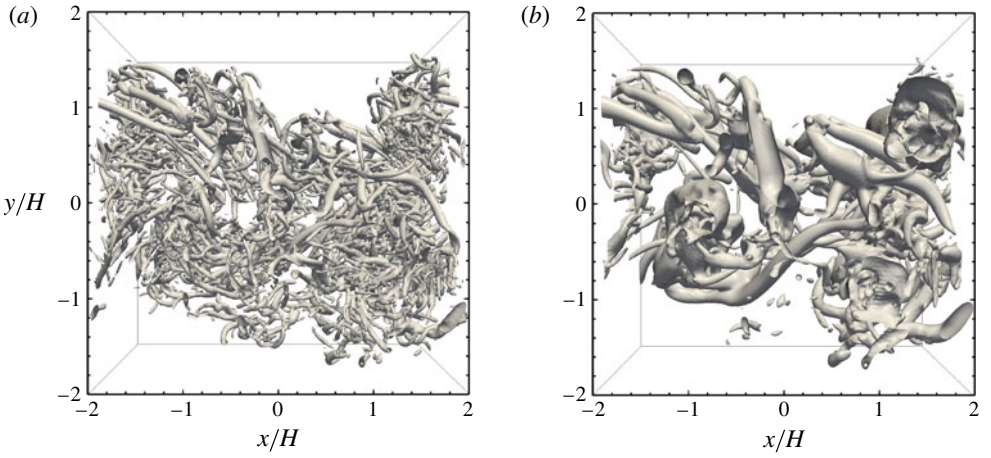

FIGURE 1. Iso-surfaces of $Q = 30(U_1/H)^2$ (*a*) and pressure $p = -0.1(\rho U_1^2)$ (*b*) at the self-similar regime ($T/T_{ref} \approx 22$). Note that the figures do not show the total extent of the lateral domain.

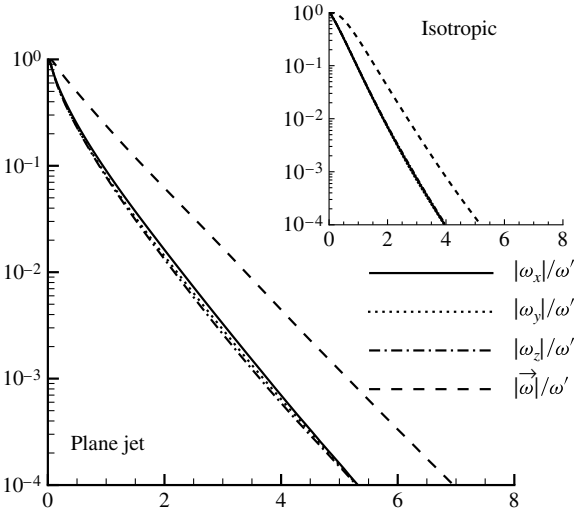

FIGURE 2. One-dimensional histograms of the volume fraction occupied by points above a certain vorticity threshold in isotropic turbulence (HIT) and in the plane jet (P. Jet). The x-axis represents, e.g. $|\omega_x|/\omega'$ with $\omega' = (\omega_i'\omega_i')^{1/2}$, where ω_i' is the fluctuating vorticity field. For the jet case ω' is roughly constant inside the shear layer and a mean value was taken.

enstrophy associated with points above a given threshold. These histograms are displayed in figure 2. In HIT the histograms for the three vorticity components are equal, which is a consequence of the statistical isotropy of the vorticity field. The same occurs in the plane jet for vorticity values corresponding to the most frequent events, e.g. $|\omega_x|/\omega' < 1$, and also, approximately, for the intense vorticity, e.g. $|\omega_x|/\omega' > 1$.

3. The intense vorticity structures inside the shear layer region

In the present work the statistics of the IVSs such as their core radius R and maximum tangential velocity u_0 were determined using a tracking procedure which is similar (with some modifications) to the procedure described by Jiménez *et al.* (1993) and Jiménez & Wray (1998). Similar vortex tracking algorithms were used in the study of the IVSs in a variety of different flows (e.g. Kida & Miura 1998; Tanahashi *et al.* 2001). The procedure used here is described in the Appendix. In (forced) isotropic turbulence Jiménez *et al.* (1993) and Jiménez & Wray (1998) showed that the vortex core size R, maximum axial vorticity ω_0, circulation Reynolds number $Re_\Gamma = \Gamma/\nu$, and maximum azimuthal velocity u_0 for the IVSs scale as $R \sim 5\eta$, $\omega_0 \sim \omega' Re_\lambda^{1/2}$, $Re_\Gamma \sim 20 Re_\lambda^{1/2}$, and $u_0 \sim u'$, respectively, where Γ is the circulation, and $\sigma_0 = (\omega_i \omega_j S_{ij}/\omega_k \omega_k)_0$ is the axial stretching rate at the axis of the IVS. It has been shown, moreover, that in forced isotropic turbulence the mean radius of the IVSs is $R \approx R_B$, where $R_B = 2(\nu/\sigma_0)^{1/2}$ is the Burgers radius, i.e. the IVSs from forced isotropic turbulence are approximately equilibrium Burgers vortices Jiménez & Wray (1998).

Table 1 presents a compilation of the IVS characteristics found in several different flows at several Reynolds numbers, such as (forced and decaying) homogeneous isotropic turbulence, homogeneous shear, mixing layer, round and plane jets, circular duct, and channel and boundary layer flows. The results obtained with the present tracking procedure in the turbulent plane jet (P. Jet) and in (forced) isotropic turbulence (HIT) are also shown.

The values of the mean radius of the vortex core divided by the Kolmogorov micro-scale $\langle R \rangle/\eta$ are close to $\langle R \rangle/\eta \approx 4$–$5$ for a variety of turbulent flows and for a wide range of Reynolds numbers. For the present HIT and P. Jet we obtain $\langle R \rangle/\eta = 4.6$ for $Re_\lambda = 111$ and 120, respectively, which is well within the range of values found in the literature. The mean tangential velocity $\langle u_0 \rangle$ divided by the root-mean-square velocity u' obtained in the literature varies as $0.50 < \langle u_0 \rangle/u' < 1.21$ indicating that $u_0 \sim u'$. We have 0.68 and 0.76 for HIT and for P. Jet, respectively, which are again well within the values found in the literature. The same is true for the mean tangential velocity normalized by the Kolmogorov velocity scale u_η. Finally, the mean axial vorticity of the IVSs can be compared by computing the Reynolds number based on the vortex circulation $Re_\Gamma = \Gamma/\nu$, divided by the square root of the Reynolds number based on the Taylor micro-scale $Re_\lambda^{1/2}$, where the circulation is obtained through $\Gamma = \oint \vec{u} \cdot \mathrm{d}\vec{l} = 2\pi R u_0$. Once more, the present values of $Re_\Gamma/Re_\lambda^{1/2} = 28.8$ (HIT) and 28.3 (P. Jet) are in good agreement with the values obtained in the literature $10.5 < Re_\Gamma/Re_\lambda^{1/2} < 32.4$. The same can be said of the axial vorticity which is $\omega_0/(\omega' Re_\lambda^{1/2}) = 0.39$ in the forced isotropic turbulence configuration and $\omega_0/(\omega' Re_\lambda^{1/2}) = 0.38$ in the turbulent plane jet, and that compares well with $0.30 < \omega_0/(\omega' Re_\lambda^{1/2}) < 0.42$ observed in isotropic turbulence in Jiménez & Wray (1998). These results show that the tracking procedure used here is indeed well implemented.

In order to compare the characteristics of the IVSs in isotropic turbulence with the IVSs in the turbulent plane jet figure 3(*a–d*) show the probability density functions (p.d.f.s) of the vortex radius non-dimensionalized by the Kolmogorov micro-scale η, the tangential velocity non-dimensionalized by the root-mean-square velocity u', the circulation Reynolds number normalized with the Reynolds number and the vortex core radius normalized with the Burgers radius, respectively.

https://doi.org/10.1017/jfm.2011.296 Published online by Cambridge University Press

Flow	Source	Re_λ	$\langle R\rangle/\eta$	$\langle R/R_B\rangle$	$\langle u_0\rangle/u'$	$\langle u_0\rangle/u_\eta$	$Re_\Gamma/Re_\lambda^{1/2}$
F. Isotropic:	Jiménez *et al.* (1993)	36–168	3.8–4.2	—	—	—	16.5–21.1
	Jiménez & Wray (1998)	37–168	4.8–4.9	0.92–1.05	0.86–0.99	—	—
	Kida & Miura (1998)	46	3.2–3.8	—	—	—	14.7–32.4
	present HIT	111	4.6	0.99	0.68	9.0	28.8
D. Isotropic:	Jiménez & Wray (1998)	62	4.8	0.82	1.21	—	—
H. Shear:	Kida & Miura (1998)	—	4.9–5.2	—	—	—	—
M. Layer:	Tanahashi *et al.* (2001)	80–100	4.5	—	0.50	—	—
Duct:	Mouri, Houri & Kawashima (2007)	719–1934	5.5–6.2	1	0.59–0.64	8.7–14.0	10.5–12.3
B. layer:	Mouri *et al.* (2007)	332–1304	5.2–6.2	1	0.68–0.82	7.6–12.8	13.6–13.7
Channel:	Kang *et al.* (2008)	200–380	4.0–5.0	—	—	1.2–2.0	—
R. jet:	Ganapathisubramani *et al.* (2008)	150	3.0–7.5	—	—	—	—
P. jet:	da Silva & Pereira (2008)	120	4.6	0.97	0.76	7.15	28.3

TABLE 1. Characteristics of the IVSs in several flows at several Reynolds numbers: forced isotropic turbulence (F. Isotropic), decaying isotropic turbulence (D. Isotropic), homogeneous shear (H. Shear), mixing layer (M. Layer), round and plane jets, (R. jet, P. jet) circular duct (Duct), channel and boundary layer flows (Channel, B. Layer). Mean values of radius R, azimuthal velocity u_0 and Reynolds number based on the circulation $Re_\Gamma = \Gamma/\nu$ for the IVSs, non-dimensionalized by the Reynolds number based on the Taylor micro-scale Re_λ, Kolmogorov micro-scale η, Burgers vortex radius R_B, Kolmogorov velocity scale u_η and root-mean-square velocity u'. The Reynolds numbers in Kang *et al.* (2008) were estimated from the data presented in the paper. Note that the definition for $Re_\Gamma = \Gamma/\nu$ used here is slightly different to the definition used by some authors where $Re_\Gamma = \Gamma/(2\pi\nu)$. In these cases the values found in the literature were converted to the definition of Re_Γ used here. For the P. Jet configuration the reference u', λ and η are taken from the conditional mean profiles of these quantities, and each instantaneous field uses its corresponding reference values for λ, u' and η which are roughly constant deep inside the turbulent region and subjected to small changes for the $N_T = 11$ fields used here.

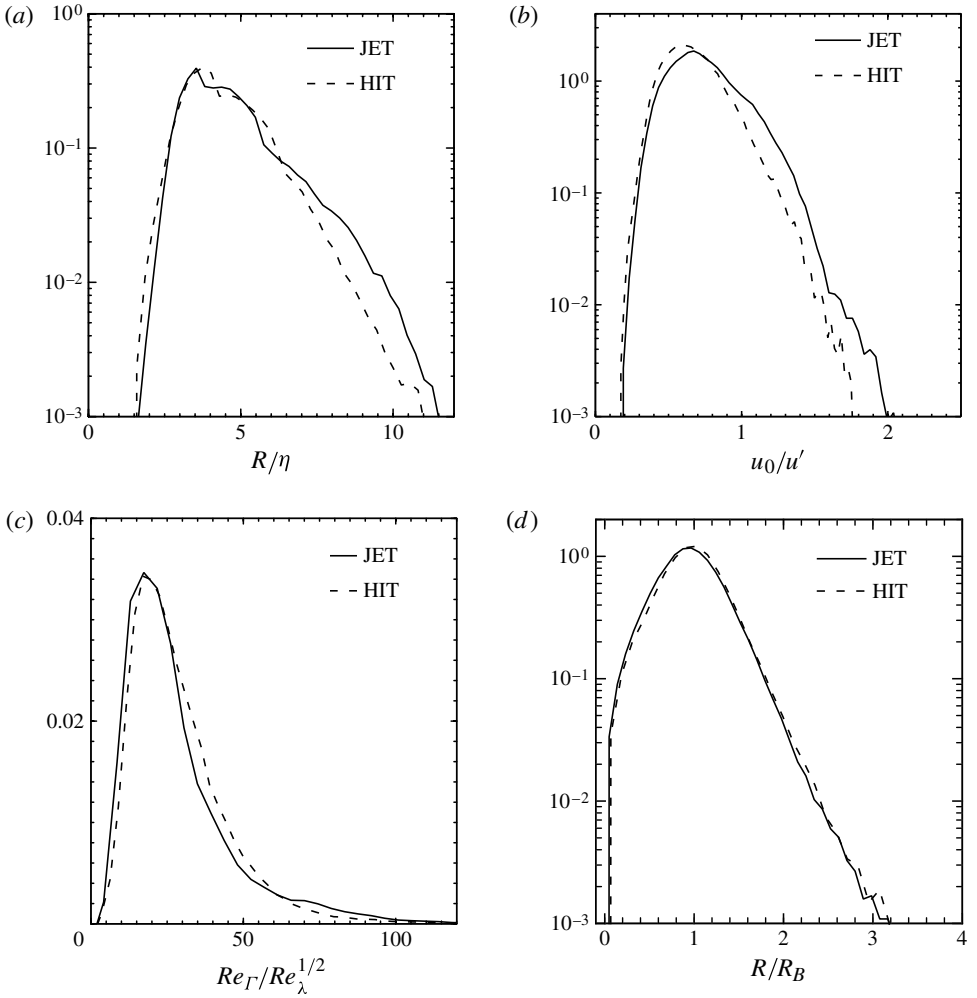

FIGURE 3. Probability density functions of the filament properties in HIT and in the P. Jet (data from the entire shear layer region): (*a*) radius normalized with the Kolmogorov micro-scale; (*b*) maximum tangential velocity normalized with the root-mean-square velocity; (*c*) circulation Reynolds number normalized with the Taylor-scale Reynolds number; (*d*) radius normalized with the Burgers radius. For the P. Jet the values used in the normalization, e.g. u', are the values deep inside the shear layer and each instantaneous field is normalized by its corresponding value of u'.

The shape and the magnitude of the p.d.f.s shown in figure 3(*a–d*) agree remarkably well with the same p.d.f.s displayed in, e.g. Jiménez *et al.* (1993) and Jiménez & Wray (1998) and in Tanahashi *et al.* (2001). Note, however, that tails of the p.d.f.s in the P. Jet show some differences compared with isotropic turbulence, e.g. the probability of finding vortex core radius with $R = 10\eta$ is slightly higher in a jet than in isotropic turbulence (figure 3*a*). Also, the extreme values of the tangential velocities found in the jet are also slightly more frequent than in isotropic turbulence (figure 3*b*). It is interesting to note that the p.d.f. of R/R_B is very similar in a jet and in isotropic turbulence which indicates that the IVSs found in the jet are well described by the Burgers vortex model. The Burgers vortex model occupies an important place in the

study of vortical structures in turbulent flows since it is known from Jiménez & Wray (1998) that the 'worms' from forced isotropic turbulence are very well described by this model.

The steady Burgers vortex is an exact solution of the Navier–Stokes equations describing a vortex tube immersed in an axisymmetric, irrotational field (Davidson 2004). In this model vortex the axial vorticity is given by

$$\omega_z(r) = \frac{\alpha\Gamma}{4\pi\nu}\mathrm{e}^{-r^2/R_B^2} \tag{3.1}$$

and the velocity field in cylindrical coordinates is

$$u_z = \alpha z, \quad u_r = -\frac{1}{2}\alpha r, \quad u_\theta = \frac{\Gamma}{2\pi r}(1-\mathrm{e}^{-r^2/R_B^2}), \tag{3.2}$$

where $\Gamma = 2\pi\int_0^\infty \omega_z(r) r\,\mathrm{d}r$ is the vortex circulation, α is the rate of strain and $R_B = 2(\nu/\alpha)^{1/2}$ is the radius of the Burgers vortex, which is kept constant due to the balance between the axial stretching rate and the radial viscous diffusion. Jiménez & Wray (1998) showed that the axial stretching in forced isotropic turbulence originates in the background vorticity consisting of structures for which $\omega' < \omega < \omega_{ivs}$. In this flow the Burgers vortex radius is $R_B = 2(\nu/\sigma_0)^{1/2}$ where $\sigma_0 = \vec{\omega}_0{}^{\mathrm{T}} \cdot \boldsymbol{S} \cdot \vec{\omega}_0 / |\vec{\omega}_0|^2$ is the axial stretching rate acting on the axis of each IVSs (with axial vorticity $\vec{\omega}_0$) and $\boldsymbol{S}$ is the local rate of strain. The ratio between the vortex core radius and the Burgers radius R/R_B in table 1 shows that in our (forced) isotropic turbulence $\langle R/R_B\rangle = 0.99$ which is very close to the values obtained by Jiménez & Wray (1998). For the plane jet we have $\langle R/R_B\rangle = 0.97$ which is slightly less than in isotropic turbulence but somehow also supports the idea that the IVSs from the planar jet are, generally (i.e. in the whole shear layer), well described by the equilibrium Burgers vortex model.

4. The intense vorticity structures near the T/NT interface

4.1. *Topology of the IVSs near the T/NT interface*

We now turn to the analysis of the IVSs near the T/NT interface. It is instructive to have a glimpse of these structures near the T/NT interface. Before we can do this the exact location of the interface separating turbulent and irrotational flow has to be defined. Since the T/NT interface divides the flow into a rotational (turbulent) and an irrotational (non-turbulent) region, the vorticity (or the enstrophy) is the appropriate variable to define the exact location of the interface. Following several previous works (e.g. Bisset *et al.* 2002; Mathew & Basu 2002; da Silva & Pereira 2008; da Silva 2009) we define the T/NT interface location as the flow surface where the local vorticity norm $\omega = (\omega_i\omega_i)^{1/2}$ is equal to a certain threshold. Recently Anand, Boersma & Agrawal (2009) compared several different criteria to define the T/NT interface.

Figures 4(*a–d*) and 5(*a–d*) show the flow structures near the T/NT interface in the upper shear layer of the plane jet allowing us to better understand the geometry and interplay of the various structures. Figure 4(*a*) displays the IVSs (yellow iso-surfaces) in sections of small circular discs, where the radius of each disc is the exact radius of the local IVSs radius computed with the vortex tracking algorithm used here. The length and radial dimension of the IVSs is not uniform but the majority of the structures seem to display similar characteristics. The IVSs do not show a clear spatial orientation, as in isotropic turbulence, but seem to be clustered into two separate regions, at the borders of the flow domain. Figure 4(*b*) shows iso-surfaces of intense enstrophy (blue) corresponding to the background vorticity, i.e. structures for which

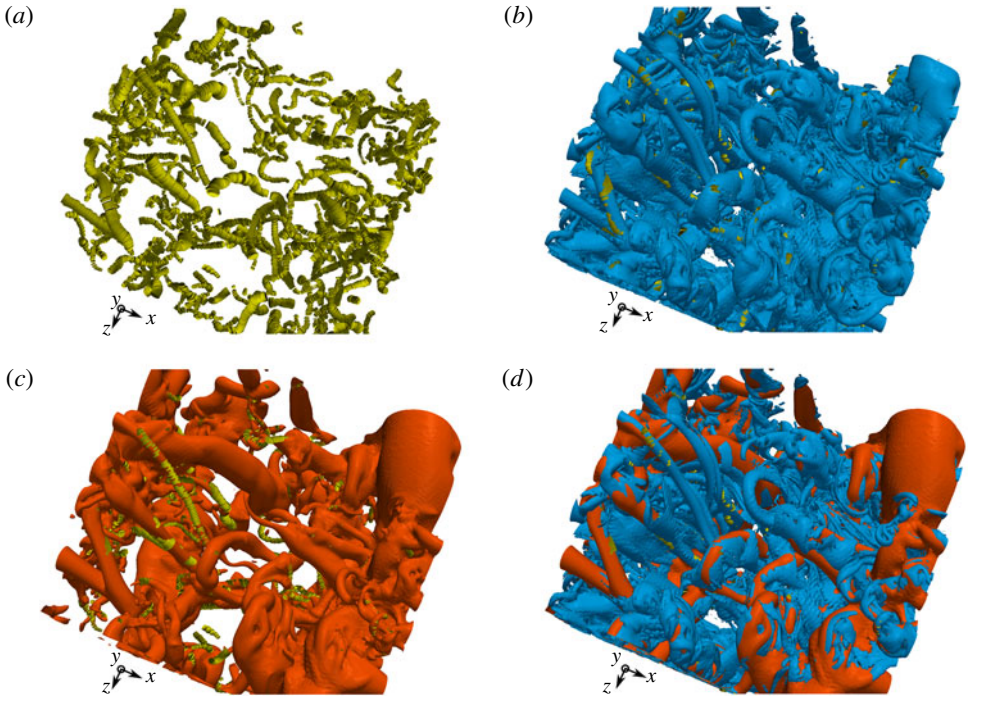

FIGURE 4. Side view of the coherent structures near the T/NT interface in the upper shear layer of the turbulent plane jet: (*a*) iso-surfaces of the IVSs detected by the vortex tracking algorithm described in the Appendix (yellow). Note that the displayed radii of the IVSs structures corresponds to the exact radius computed with the vortex tracking algorithm; (*b*) iso-surfaces of enstrophy (blue) and IVSs (yellow); (*c*) iso-surfaces of low-pressure regions (orange) and IVSs (yellow); (*d*) iso-surfaces of low-pressure regions (orange), strong enstrophy (blue) and IVSs (yellow). Colour references apply to the online version.

the enstrophy is $\omega' < \omega < \omega_{ivs}$ and IVSs (yellow). As can be seen the IVSs merge with the background vorticity indicating that the IVSs are extreme events of the background vorticity, as is the case in isotropic turbulence, as described by Jiménez *et al.* (1993). The longer enstrophy structures seem to consist of pairs of vortices aligned preferentially with the streamwise direction. Figure 4(*c*) shows iso-surfaces of low-pressure regions (orange) and IVSs (yellow). The pressure field allows one to observe the large-scale structures of the flow showing three large-scale structures, aligned with the z direction: two at the upper shear layer, at the extremes of the domain, and another one below, at the lower shear layer. A considerable number of streamwise structures are also observed. The radius of the spanwise rollers R_{lvs} was estimated by da Silva & Taveira (2010) and is close to the Taylor micro-scale $R_{lvs} \sim \lambda$. The structures are remnants of the Kelvin–Helmholtz rollers that are known to arise during the early stages of the transition to turbulence in a jet. Comparing figure 4(*a*,*c*) one sees that the clusters of IVSs described before are located inside the large-scale vortices identified by the low-pressure iso-surfaces, however the correlation between the large-scale structures and the IVSs is apparently low, which underscores the scale separation between the two types of structure. Finally, figure 4(*d*) shows all three iso-surfaces, i.e. IVSs (yellow), enstrophy (blue) and pressure (orange), and shows that there is some overlap between the enstrophy structures and the pressure but

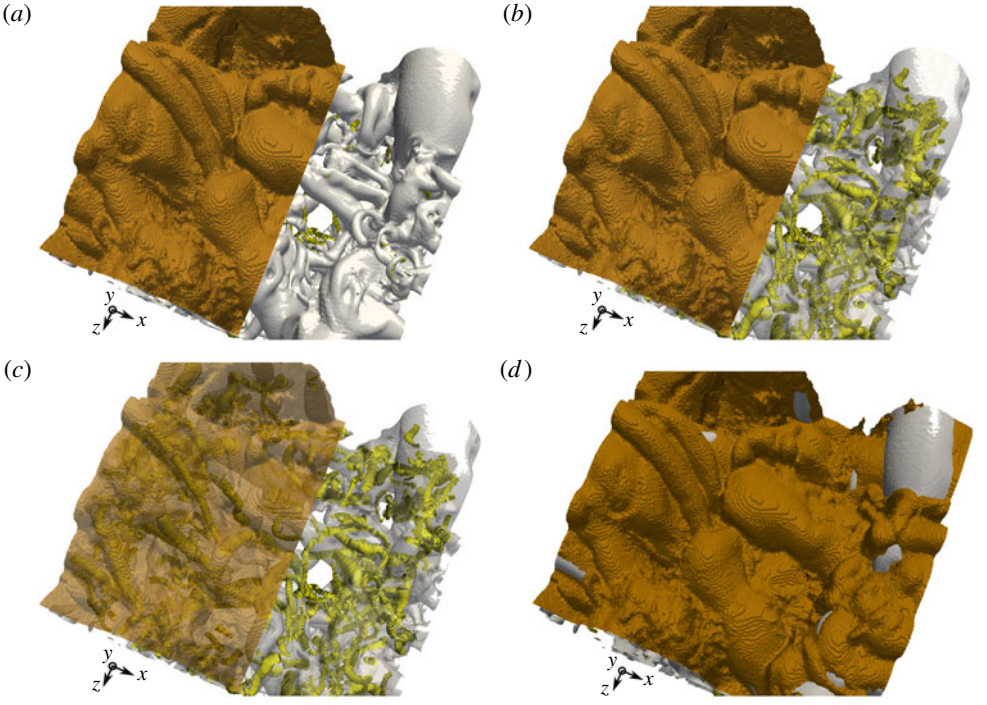

FIGURE 5. Side view of the coherent structures near the T/NT interface in the upper shear layer of the turbulent plane jet: (*a*) iso-surfaces of the IVSs (yellow), low-pressure regions (white), and the T/NT interface (brown); (*b*) same as in (*a*) but using a transparent iso-surface for the pressure; (*c*) same as in (*b*) but using a transparent iso-surface for the T/NT interface; (*d*) iso-surfaces of low-pressure regions (orange), and the T/NT interface (brown). Colour references apply to the online version.

only for the bigger enstrophy structures, such as one of the two streamwise vortices which seem to be merging into a single structure (compare also figure 4*b*,*c*), i.e. the spatial overlap between the LVSs and the IVSs (low pressure is associated with strong vorticity) is clearly apparent from the figure, but one can again see that the IVSs exhibit more 'random' spatial orientation than the LVSs.

In order to analyse the interplay between these structures and the T/NT interface figure 5(*a–d*) use partially transparent (or translucent) iso-surfaces of the same quantities displayed in figure 4(*a–d*) and show also the T/NT interface at the upper shear layer of the jet. As in several works, e.g. Bisset *et al.* (2002), Mathew & Basu (2002) and da Silva (2009), the T/NT interface consists on the surface defined by a certain vorticity norm threshold $\omega = (\omega_i\omega_i)^{1/2}$, where $\omega_i = \nabla \times u_i$ is the vorticity field and the detection threshold is $\omega = 0.7U_1/H$, which is the same threshold used in Bisset *et al.* (2002) and Mathew & Basu (2002). Figure 5(*a*) shows part of the T/NT interface (brown) and the LVSs (white) identified using pressure iso-surfaces, as well as some IVSs (yellow). The T/NT interface is strongly convoluted, something that has been well known for a long time, and one sees immediately that the length scale of the convolutions is very similar to the length scale of the LVSs below its surface. Figures 5(*b*) and 5(*c*) are equivalent to figure 5(*a*) but show the pressure iso-surface as translucent (figure 5*b*) and the T/NT interface as translucent (figure 5*c*) which allows one to observe the IVSs below the T/NT interface. In contrast to the LVSs, the IVSs

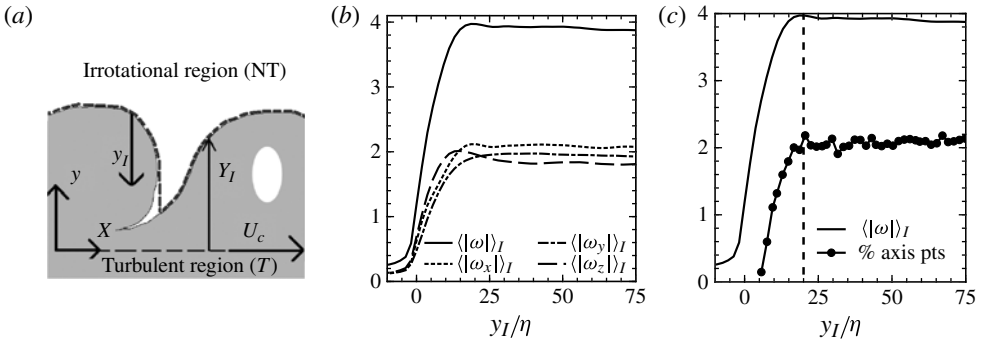

FIGURE 6. (*a*) Sketch of the T/NT interface indicating the vorticity surface (solid line) and the interface envelope position Y_I (dashed line), with the coordinate system of the plane jet (x, y) and that used in the conditional statistics (y_I). The 'hole' represents a region of irrotational fluid inside the turbulent region and is removed from the statistical sample. (*b*) Mean conditional profiles of $\langle|\omega|\rangle_I$, $\langle|\omega_x|\rangle_I$, $\langle|\omega_y|\rangle_I$ and $\langle|\omega_z|\rangle_I$ (all normalized by U_1/H). (*c*) Percentage of the total number of points identified as IVSs, as a function of the distance from the T/NT interface in the region $0 < y_I/\eta < 75$, i.e. integrating this profile in $0 < y_I/\eta < 75$ we have 100 % ($\langle|\omega|\rangle_I$ is also shown). The vertical dashed line at $y_I/\eta = 20$ is one Taylor micro-scale from the T/NT interface.

play no role on the definition of the T/NT interface characteristics, since they are neither of the same scale of the observed T/NT interface convolutions nor are they the first structures that appear right below the T/NT interface. With figure 5(*d*) displaying the full T/NT interface at the upper shear layer one realizes, not surprisingly, that the observed convolutions of the T/NT interface are dictated by the LVSs underneath its surface. Indeed the T/NT interface coincides with the physical line defined by the LVSs at the edge of the upper shear layer and this fact underlines one of the well-known features of the T/NT interface that has been known for some time (e.g. Townsend 1976): the LVSs are responsible for the observed convolutions of the T/NT interface and this explains why the length scale of these convolutions is roughly equal to the length scale of the LVSs.

4.2. *Conditional statistics of the IVS characteristics near the T/NT interface*

In order to study the influence of the T/NT interface upon the IVS characteristics we use conditional statistics in relation to the distance from the T/NT interface. The procedure used to obtain these statistics has been used in several previous works (e.g. Bisset *et al.* 2002; Westerweel *et al.* 2005, 2009; da Silva & Pereira 2008; da Silva 2009), and is briefly outlined here since it was already described in detail in da Silva & Pereira (2008) and da Silva (2009).

The sketch in figure 6(*a*) shows the T/NT interface separating the turbulent and the irrotational flow regions at the upper shear layer of the plane jet. As described before in the present work the T/NT interface location $Y_I(x)$ is defined using the vorticity norm $\omega = (\omega_i\omega_i)^{1/2}$. The envelope location $Y_I(x)$ is determined using a linear interpolation along the y direction, for each one of the N_x grid points along the x direction in the original coordinate system. Once the T/NT interface location $Y_I(x)$ has been determined a new local coordinate system y_I is defined to be right at the interface location and the conditional statistics are made in this local coordinate system. The T/NT interface is at $y_I = 0$, while the irrotational and turbulent regions are defined by $y_I < 0$ and $y_I > 0$, respectively. We denote these conditional statistics

by $\langle\rangle_I$. Re-entrant zones are handled as in, e.g. Westerweel *et al.* (2009) (see figure 6*a*). 'Holes' of 'ambient fluid' that appear inside the jet are removed from the statistical sample. Note that here, as in da Silva (2009), the local coordinate system is always aligned with the y direction, unlike in da Silva & Pereira (2008) where the conditional statistics were made along a line which is always locally normal to the T/NT interface. It was observed that both procedures lead to very similar results, however. The same procedure is used also for the lower shear layer and the statistics use each one of the N_z spanwise planes and $N_T = 11$ instantaneous fields taken from the fully developed turbulent regime between $T/T_{ref} = 20.2$ and 27.0. Note that the conditional profiles shown below highlight the region in the proximity of the T/NT interface, in $0 < y_I/\eta < 75$, since the variables analysed here are roughly constant from $y_I/\eta \approx 75$ until the centre of the jet shear layer, which is located approximately at $y_I/\eta \approx 140$–150. Some of the conditional mean profiles presented in this work are scaled by reference turbulent quantities, e.g. $\langle R\rangle_I/\eta$. Although in general these quantities, e.g. η or u', vary in time and along the y direction, their conditional mean profiles roughly collapse deep inside the turbulent region for the $N_T = 11$ fields used here. Nevertheless the reference turbulent quantities used for each field correspond to their value deep inside the turbulent region, e.g. for each field/instant η is taken as $\eta = \langle\eta\rangle_I$ for $y_I/\eta = 75$. The conditional mean profiles result from averaging all of the instantaneous profiles, where each one was scaled by its 'instantaneous' reference quantity, i.e. $\langle R/\eta\rangle_I = \langle R(y_I)/\eta\rangle_I = 1/N_T \sum_{i=1}^{N_T=11} \langle R\,(y_I)\rangle_I\,/\eta_i$. Since the turbulence fields are from the self-similar turbulent regime we assume that the turbulent characteristics studied here are representative of the flow in turbulent jets.

Figure 6(*b*) shows conditional mean profiles of $\langle|\omega_x|\rangle_I$, $\langle|\omega_y|\rangle_I$ and $\langle|\omega_z|\rangle_I$ in relation to the distance from the T/NT interface, showing a sharp jump across the T/NT interface with thickness roughly equal to 20η. In the present simulation and deep inside the turbulent region we have $\lambda \approx 20\eta$, where λ is the Taylor micro-scale, therefore this jump is equal to the Taylor micro-scale, in agreement with other experimental and numerical works (Bisset *et al.* 2002; Westerweel *et al.* 2005). As described in the introduction and as shown by da Silva & Taveira (2010) this is because the thickness of the T/NT interface is equal to the radius of the LVSs near the T/NT interface $\delta_\omega \approx R_{lvs}$.

Figure 6(*c*) shows the percentage of points which were identified as belonging to an existing IVS axis in the region $0 < y_I/\eta < 75$, i.e. the fraction of the total number of detected IVSs in this region, as function of the distance from the T/NT interface (integrating this profile in $0 < y_I/\eta < 75$ we have 100 %). For $y_I/\eta > 20$–25 this number is roughly constant, but it decreases sharply as one approaches the T/NT interface until, for $0 < y_I/\eta < 5$, this number is negligibly small. This shows, as expected, that there is a thin region near the T/NT interface where no axis from IVSs exist, since this is roughly the radius of the existing IVSs. This agrees also with the results of da Silva & Taveira (2010) and da Silva & dos Reis (2011): the T/NT interface in fact consists of (or is made up from) LVSs sitting at that location. Finally, note that (figure 6*c*) the size of the adjusting region $5 < y_I/\eta < 25$ where the IVSs are not as numerous as inside the jet is consistent with the analysis of the invariant maps described by da Silva & Pereira (2008, 2009): at $y_I/\eta = 20$ there are already signs of the presence of LVSs.

4.3. *IVS characteristics near the T/NT interface: the Burgers vortex model*

In this section we analyse the IVS characteristics as function of the distance from the T/NT interface. Figure 7(*a–d*) show conditional mean profiles of the vortex core

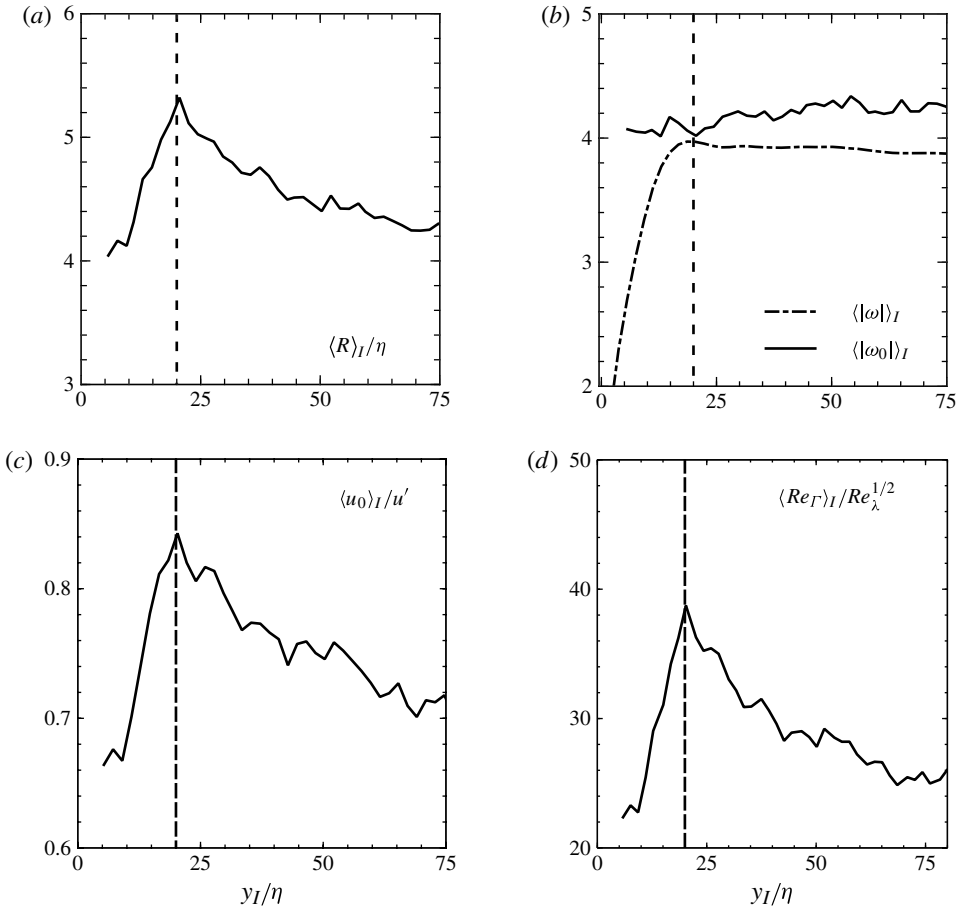

FIGURE 7. Conditional profiles of IVS characteristics: (*a*) vortex core radius $\langle R\rangle_I/\eta$; (*b*) axial vorticity $\omega_0(U_1/H)$ (the vorticity norm from the whole field $|\omega|$ is also shown); (*c*) tangential velocity $\langle u_0\rangle_I/u'$; (*d*) circulation Reynolds number $\langle Re_\Gamma\rangle_I/Re_\lambda^{1/2}$. The vertical dashed line at $y_I/\eta = 20$ is one Taylor micro-scale from the T/NT interface.

radius R (figure 7*a*), axial vorticity ω_0 (figure 7*b*), azimuthal velocity u_0 (figure 7*c*) and circulation Reynolds number (figure 7*d*). The conditional mean profile of the vorticity norm $|\omega|$ for the whole flow field is also shown (figure 7*b*). The vertical dashed line at $y_I/\eta = 20$ marks the distance from the T/NT interface which is equal to the Taylor micro-scale.

The core radius deep inside the jet shear layer ($y_I/\eta > 75$) is equal to $\langle R\rangle_I \approx 4.3\eta$ which is close to the value observed in isotropic turbulence. However, it increases near the T/NT interface reaching $\langle R\rangle_I \approx 5.3\eta$ at $y_I/\eta \approx 20$, before decreasing to $\langle R\rangle_I \approx 4.2\eta$ at $y_I/\eta = 10$. It is interesting to see that the maximum observed radius is located at $y_I/\eta \approx 20$ which is exactly one Taylor scale from the T/NT interface and is also the point of maximum vorticity as described by da Silva & Pereira (2008). This can be explained by the dynamics of the IVSs near the jet edge as will be described below. The quick drop of $\langle R\rangle_I/\eta$ in the region $10 < y_I/\eta < 20$ has to be caused by the lack of space inside this layer. There is simply no space for IVSs, whose diameter is close to 10η, inside this region. Note that as we saw before the number of detected IVSs

in $0 < y_I/\eta < 20$ drops fast as the T/NT interface is approached and therefore the statistics from this region have to be considered carefully even though the observed trend is clear.

Interestingly the axial vorticity of the detected IVSs is sensibly constant throughout the jet shear layer (figure 7*b*), so that even the IVSs very close to the T/NT interface have similar axial vorticity to those found deep inside the shear layer. This indicates that it is mostly the orientation of the IVSs and not their vorticity magnitude that is affected by the presence of the T/NT interface, in agreement with da Silva & dos Reis (2011) who showed that the IVSs close to the T/NT interface tend to be aligned with the tangent to the interface surface.

The evolution of the conditional azimuthal velocity of the IVSs (figure 7*c*) resembles the evolution of R/η with a maximum close to the T/NT interface $\langle u_0\rangle_I/u' \approx 0.84$ (at $y_I/\eta = 20$) and smaller values deep inside the shear layer $\langle u_0\rangle_I/u' \approx 0.72$ for $y_I/\eta > 75$. Again, very close to the T/NT interface $10 < y_I/\eta < 20$ the azimuthal velocity of the IVSs decreases very fast, which indicates that the vortex filament characteristics are modified by the presence of the T/NT interface.

Although the IVSs are a particular subset of structures taken from a sea of different eddy sizes we can already draw one conclusion from the above results: since the core radius and azimuthal velocity are higher near the T/NT interface ($y_I/\eta \approx 20$) than in the region $10 < y_I/\eta < 20$, and than deep inside the turbulent region ($y_I/\eta > 75$), while the axial vorticity is roughly constant across the shear layer, this implies that the circulation Γ_0 of the IVSs is also maximum at $y_I/\eta \approx 20$ and has lower values in $10 < y_I/\eta < 20$ and in the interior of the shear layer $y_I/\eta > 20$, because the circulation of each particular IVSs is $\Gamma_0 \approx 2\pi u_0 R$. This is indeed what is observed in the circulation Reynolds number whose conditional profile is shown in figure 7(*d*).

It is tempting to infer that the observed differences in the circulation of the IVSs across the shear layer are caused by the characteristics of the flow field near the T/NT interface since the results suggest that the IVSs that are to be found at this location were formed at that particular location and are not structures that were formed in other parts of the flow, e.g. the jet centreline, and that were simply advected into the jet edge. Although only a detailed analysis of the IVSs in time would allow us to settle these questions definitively, it is easy to show that the lifetime of the IVSs, T_τ, is much smaller than the time needed for these structures to travel from the region near the jet centreline into the region near the jet edge T_V. As we show in § 4.4, the characteristic time associated with the downstream convection of the IVSs, T_U, is much bigger than the lifetime of these structures $T_\tau \ll T_U$, and since the downstream transport, associated with the higher mean velocity component of the jet, is much smaller than the time associated with lateral transport of the IVSs, it follows naturally that the IVSs are dissipated much faster than they can be transported from the centre of the jet into the region near the jet edge, i.e. $T_\tau \ll T_U \ll T_V$.

The dynamics of the IVSs can be analysed by comparing their characteristics with the Burgers vortex model. As described above it is well known that the Burgers vortex model provides an excellent description of the IVSs found in (forced) isotropic turbulence and it is expected that this model will provide a good description for the IVSs in free shear flows, e.g. jets, since the IVSs are similar in many different flows. The mean value of R/R_B for the entire shear layer supports this view with $\langle R/R_B\rangle = 0.97$ (see table 1). In forced isotropic turbulence Jiménez & Wray (1998) observed that the radius of the IVSs is equal to the Burgers radius $R = R_B$ for a wide range of Reynolds numbers: $0.96 < R/R_B < 1.05$ for $62 < Re_\lambda < 168$. However, in decaying isotropic turbulence Jiménez & Wray (1998) observed $R/R_B = 0.82$ for

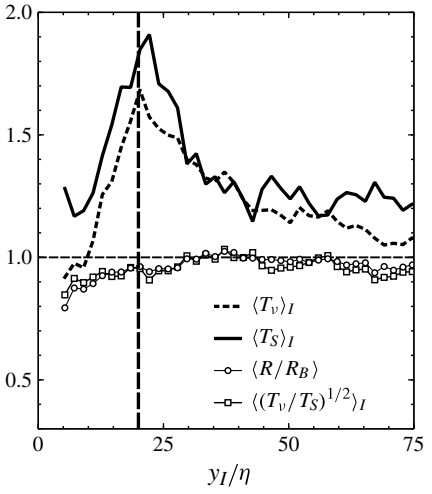

FIGURE 8. Conditional profiles of diffusion and stretching time scales $\langle T_\nu \rangle_I$ and $\langle T_S \rangle_I$, and ratio between the local vortex core radius and the Burgers radius $\langle R/R_B \rangle_I$. The vertical dashed line at $y_I/\eta = 20$ is one Taylor micro-scale from the T/NT interface.

$Re_\lambda = 62$ showing that the Burgers vortex is a less accurate model to describe the dynamics of the IVSs in decaying turbulence. The jet flow studied here is also in some sense a decaying flow since the root-mean-square velocity decreases slowly with the axial direction (or with time in a temporal simulation) in the far field self-similar region. However, the presence of a mean shear producing turbulent kinetic energy and thus some additional local strain (compared with decaying isotropic turbulence) is expected to counter this decay to some extent. Therefore, in a jet we expect to be somehow between the classical cases of forced and decaying isotropic turbulence.

We start to analyse the dynamics of the IVSs by comparing the measured vortex core radius R of each identified structure with the local Burgers radius $R_B = 2(\nu/\sigma_0)^{1/2}$ through the ratio R/R_B displayed in figure 8. Note that R_B can only be computed for axial IVS points where vortex stretching dominates over compression $\sigma_0 > 0$. The conditional profile of $\langle R/R_B \rangle_I$ is slightly smaller than 1.0 close to the T/NT interface ($\langle R/R_B \rangle_I \approx 0.9$ in $5 < y_I/\eta < 30$), attains a maximum of around $\langle R/R_B \rangle_I \approx 1.0$ in $30 < y_I/\eta < 50$, and decreases to $\langle R/R_B \rangle_I \approx 0.97$ in the centre of the shear layer. Thus, R/R_B in the jet is indeed between the values observed in forced and in decaying isotropic turbulence. This shows that the Burgers vortex model, although being still an approximately good description for most of the IVSs in the jet, is less accurate in modelling the IVSs near the T/NT interface, and that for these IVSs (near the T/NT interface) enstrophy generation by axial vortex stretching and radial enstrophy viscous diffusion are not in perfect equilibrium, and the vortex core radius of these structures is not stable, i.e. it is evolving in time.

To investigate where this imbalance comes from we define two time scales associated with the two mechanisms: $T_S = 1/\sigma_0$ and $T_\nu = R^2/(4\nu)$ associated with axial vortex stretching and radial viscous diffusion, respectively. If the two time scales are equal $T_S = T_\nu$, the vortex core radius is equal to the Burgers radius $R = R_B = 2(\nu/\sigma_0)^{1/2}$, and the vortex core is stable, i.e. it does not change in time. If, in contrast, the two time scales are not equal the mechanism associated with the smaller time scale dominates, e.g. a vortex where $T_\nu < T_S$ is subjected to more intense

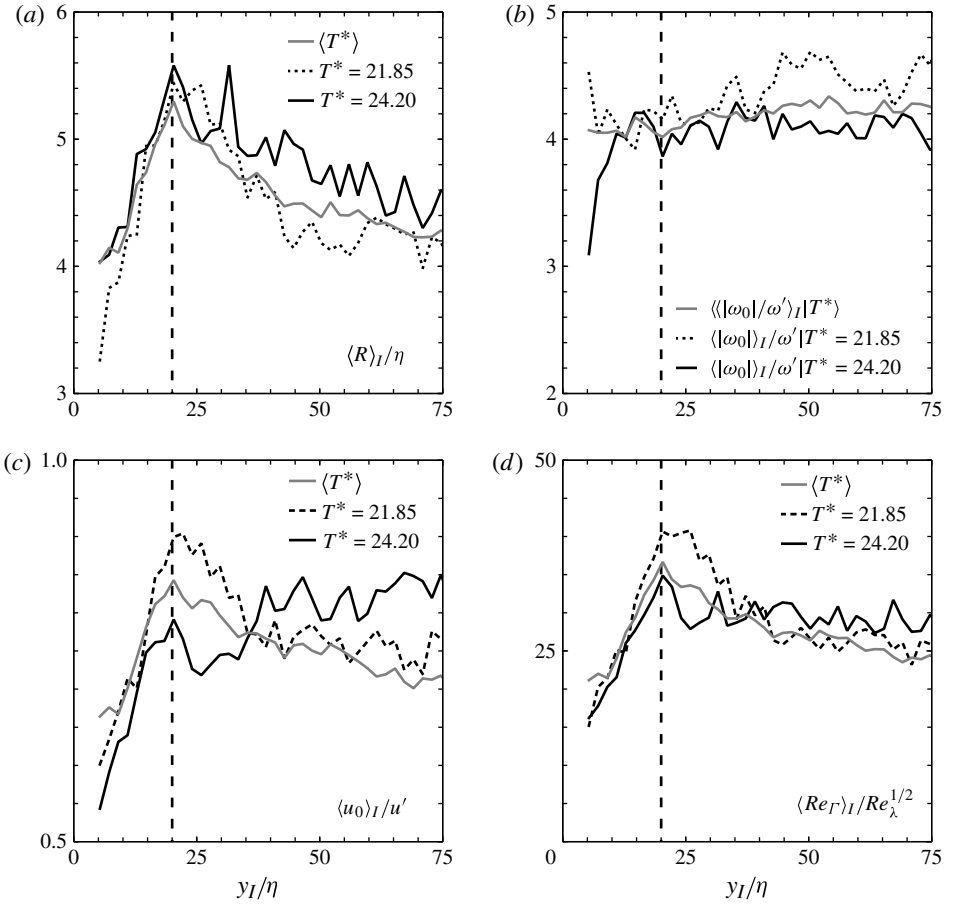

FIGURE 9. Temporal evolution of the conditional profiles of IVS characteristics, showing the values at $T/T^* \approx 22$ and $T^* \approx 24$, and the reference mean values (shown in figure 7): (*a*) vortex core radius $\langle R \rangle_I / \eta$; (*b*) axial vorticity $\langle \omega_0 \rangle_I$; (*c*) tangential velocity $\langle u_0 \rangle_I / u'$; (*d*) circulation Reynolds number $\langle Re_\Gamma \rangle_I / Re_\lambda^{1/2}$. The vertical dashed line at $y_I/\eta = 20$ is one Taylor micro-scale from the T/NT interface.

viscous diffusion than axial stretching, and this will tend to increase its radius in time. The ratio of the conditional time scales $\langle (T_v/T_S)^{1/2} \rangle_I$ displayed in figure 8 shows that this is the dynamical situation for the IVSs near the T/NT interface, and to a smaller extent to many other IVSs to the interior of the shear layer, since $\langle T_v/T_S \rangle_I < 1.0$. Note that for given σ_0 and ν, the two time scales are related to the vortex core radius by $(T_v/T_S)^{1/2} = R/R_B$, and the present results comply with this relationship (see figure 8).

Figure 9(*a–d*) show the instantaneous conditional IVS characteristics for two different times $T/T_{ref} = T^* \approx 22$ and $T^* \approx 24$ (the mean value resulting from the averaging procedure using $N_T = 11$ instantaneous fields discussed in figure 7 is also shown). This allows one to observe the temporal evolution of several IVS characteristics during a short time interval. The degree of convergence of these curves is not perfect due to the small number of samples, but is sufficient to observe the main trends. One observes that as time progresses from $T^* \approx 22$ to $T^* \approx 24$ the axial vorticity (figure 9*b*) and the tangential velocity (figure 9*c*) decrease in the majority of

the flow points, while the magnitude of the vortex core radius increases (figure 9*b*). This is exactly what one would expect in an isolated vortex if the viscous diffusion of enstrophy is more important than the axial enstrophy stretching. Note that the circulation Reynolds number also decreases (figure 9*d*). As remarked by a referee, this last result underscores the fact that the dynamics of the IVSs is not inviscid, and the circulation of the individual IVSs is not constant, but decreasing in time. This is a natural consequence of the fact that the length scale of the IVSs is of the order of the Kolmogorov micro-scale ($R \approx 4$–5η) implying that the viscosity is important for these structures.

The series of observations described above raise a new question: why is the dynamics of the IVSs different near the T/NT interface compared with deep inside the turbulent region? Specifically, we are interested in understanding what the reason is that the radii of the IVSs near the jet edge are larger than inside the rest of the shear layer. This issue is important in the context of the turbulent entrainment since the 'nibbling' eddy motions associated with the entrainment are thought to be dictated by the IVSs near the T/NT interface. It has been remarked that only vortices that are approximately described by the Burgers vortex will have long lifetimes inside a turbulent flow, i.e. long lived IVSs must have a radius close to the Burgers radius $R \approx R_B$. Therefore the key issue here seems to be the axial stretching rate σ_0 acting on the axis of the IVSs, given that ν is of course the same everywhere in the flow.

We start to investigate this issue by analysing the conditional profiles of stretching rate $\langle\sigma\rangle_I = \langle\omega_i\omega_j S_{ij}/\,(\omega_k\omega_k)\rangle_I$, and mean stretching rate $\langle\bar{\sigma}\rangle_I = \langle\omega_i\rangle_I\langle\omega_j\rangle_I\langle S_{ij}\rangle_I/\langle(\omega_k\omega_k)\rangle_I$ for the whole flow field, in figure 10(*a*). We note from the outset that the total $\langle\sigma\rangle_I$ and mean $\langle\bar{\sigma}\rangle_I$ stretching rates are very different with $\langle\bar{\sigma}\rangle_I \ll \langle\sigma\rangle_I$ which shows that the mean flow has a negligible influence on the stretching rate (for the whole flow field). Moreover, $\langle\sigma\rangle_I < 0$ is negative in the irrotational region $y_I/\eta < 0$ implying a prevalence of compression over stretching of the fluid elements as the T/NT interface is approached in agreement with da Silva & Pereira (2008), and increases sharply after the T/NT interface has been crossed displaying a peak at $y_I/\eta \approx 5$. After this $\langle\sigma\rangle \approx 0.4$ for $y_I/\eta > 30$. Since the vorticity norm $|\omega|$ is roughly constant inside the shear layer, the stretching rate must increase with y_I for $y_I > 0$ like the rate of strain, as described by da Silva & Pereira (2008), provided that the alignment between enstrophy and strain is unchanged. A relatively slow increase in the magnitude of the rate-of-strain norm near the jet edge was indeed observed independently by da Silva & Pereira (2007*b*, 2008) and Holzner *et al.* (2007), which explains that the enstrophy production increases also slowly after the T/NT interface, again as shown by da Silva & Pereira (2007*b*, 2008) and Holzner *et al.* (2007).

To analyse the stretching rate acting on the axis of the IVSs figure 10(*b*) displays conditional profiles of total axial stretching rate $\langle\sigma_0\rangle_I = \langle\boldsymbol{\omega_0}\cdot\boldsymbol{S}\cdot\boldsymbol{\omega_0}/\omega_0^2\rangle_I$, positive axial stretching rate $\langle(\sigma_0 > 0)\rangle_I$, i.e. $\langle\sigma_0\rangle_I$ for $\sigma_0 > 0$, and mean axial stretching rate $\langle\bar{\sigma_0}\rangle_I = \langle\boldsymbol{\omega_0}\rangle_I\cdot\langle\boldsymbol{S}\rangle_I\cdot\langle\boldsymbol{\omega_0}\rangle_I\,/\,\langle\omega_0^2\rangle_I$. The conditional profile of the total axial stretching rate $\langle\sigma_0\rangle_I$ accounts for both positive and negative events, associated with vortex stretching and vortex compression, respectively, while $\langle(\sigma_0 > 0)\rangle_I$ accounts only for vortex stretching, which is more important than compression, and explains the observed differences between the two curves, i.e. $\langle(\sigma_0 > 0)\rangle_I > \langle\sigma_0\rangle_I$. The contribution of the mean field gradients to the total stretching can be appreciated in $\langle\bar{\sigma_0}\rangle_I$. Unlike σ for the whole turbulent flow, σ_0 has a non-negligible influence of the mean field, as can be attested by the fact that $\langle\sigma_0\rangle_I$ and $\langle\bar{\sigma_0}\rangle_I$ have comparable magnitudes. An even more striking feature of $\langle\sigma_0\rangle_I$ as well as of $\langle\bar{\sigma_0}\rangle_I$, is that it attains its minimum right at $y_I/\eta \approx 20$, i.e. exactly at the point where the radius of the IVSs is maximum,

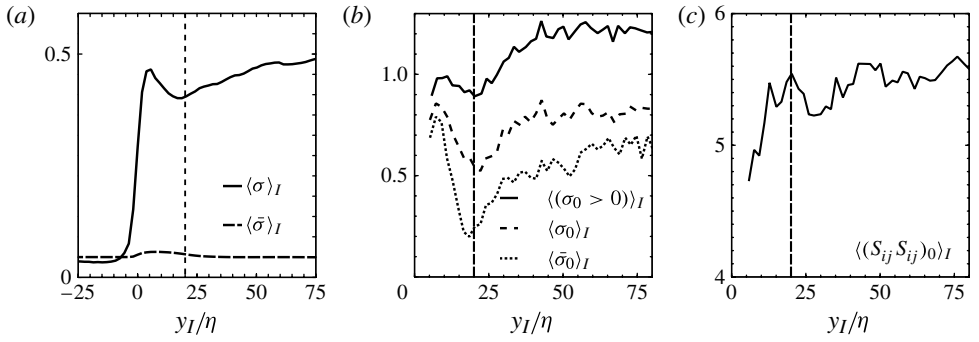

FIGURE 10. Conditional profiles of: (*a*) stretching rate $\langle\sigma\rangle_I$ and mean stretching rate $\langle\bar{\sigma}\rangle_I$; (*b*) stretching rate $\langle\sigma_0\rangle_I$, positive stretching rate $\langle(\sigma_0 > 0)\rangle_I$ and mean stretching rate $\langle\bar{\sigma_0}\rangle_I$, at the axis of the IVSs; (*c*) rate-of-strain norm at the axis of the IVSs $\langle(S_{ij}S_{ij})_0\rangle_I$. The vertical dashed line at $y_I/\eta = 20$ is one Taylor micro-scale from the T/NT interface.

indicating that the evolution of the conditional radius of the IVSs is indeed caused by the behaviour of σ_0 near the jet edge. Deep inside the turbulent region $y_I/\eta > 40$ $\langle\sigma_0\rangle_I$, $\langle\bar{\sigma_0}\rangle_I$ and $\langle(\sigma_0 > 0)\rangle_I$ are roughly constant, in contrast with the region $0 < y_I/\eta < 40$, where $\langle\sigma_0\rangle_I$ is seen to decay to its minimum.

It remains to understand what causes the decay of σ_0 near the T/NT interface, and we now turn the investigation in this direction. Here σ_0 depends on the rate of strain $(S_{ij})_0$ and on the vorticity ω_0 on the axis of the IVS, but as we have seen before ω_0 is roughly constant across the whole shear layer (see figure 7*b*). As for the strain acting on the axis of the IVS, figure 10(*c*) displaying conditional rate of strain $(S_{ij}S_{ij})_0$ on the axis of the IVS shows that this quantity alone cannot explain the observed behaviour of σ_0 at $0 < y_I/\eta < 40$, since $(S_{ij}S_{ij})_0$ at $y_I/\eta = 20$ is similar to $(S_{ij}S_{ij})_0$ for $y_I/\eta > 40$. The observed decay of $\langle\sigma_0\rangle_I$ near the T/NT interface, however, starts by $y_I/\eta \approx 40$. Recall that da Silva & Pereira (2008) and Holzner *et al.* (2007) showed that the rate of strain for the whole flow field is also roughly constant inside the turbulent region. Therefore, the decay of σ_0 around $y_I/\eta \approx 40$ has to be explained by a decrease in the alignment between ω_0 and $(S_{ij})_0$ near the jet edge. A decrease in the alignment between ω_i and S_{ij} (for the entire field) near the T/NT interface was reported in Holzner *et al.* (2007) and is consistent with the T/NT interface affecting the orientation more than the magnitude of the vorticity field described before.

There is however another explanation for the observed decay of σ_0 near the T/NT interface. Indeed it has been shown that in isotropic turbulence the axial stretching rate acting on the IVSs originates in the background vorticity structures, and these structures on the other hand lie at the borders of the weak vorticity or velocity eddy structures, which are themselves relatively free from vorticity in their centres (Jiménez & Wray 1998). If we can draw a parallel with the present jet flow, the biggest LVSs from the jet with radius of the order of the Taylor micro-scale consist of weak vorticity structures whereas the smaller LVSs are the background vorticity structures. The IVSs are then stretched in the borders of the biggest LVSs in the flow. To understand the dynamics of the eddies near the T/NT interface figure 11 shows a sketch of the flow depicting the LVSs and IVSs near the jet edge. The IVSs deep inside the shear layer are stretched by the surrounding large-scale structures, and the resulting stretching rate imposes their radius $R \sim 4.6\eta$. For the IVSs near the T/NT interface, however, only a fraction of the LVSs exist and therefore the overall

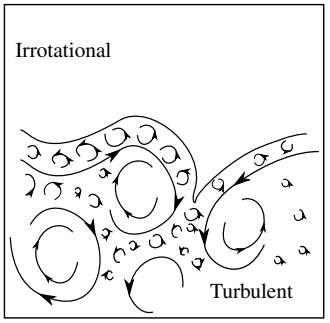

FIGURE 11. Sketch of the (small) IVSs and (big) LVSs near the T/NT interface in the jet. The T/NT interface is defined by the LVSs near the jet edge and the IVSs appear more to the interior of the jet shear layer. The average radius of the IVSs near the T/NT interface is bigger than deep inside the jet shear layer.

stretching rate on the IVSs will be smaller than inside the jet. Consequently we expect the stretching rate acting on the IVSs near the jet edge to be smaller by a factor Σ_δ than the stretching rate inside the jet $\sigma_0(y_I/\eta = \lambda) = \Sigma_\delta \sigma_0(y_I/\eta > \lambda)$, and this explains the larger IVSs found near the T/NT interface. We note that in the present results this factor is close to $\Sigma_\delta \approx 3/4$.

The picture that emerges for the IVSs in the jet is as follows: the IVSs inside the jet are approximately described by the Burgers vortex model $R \approx R_B = 2(\nu/\sigma_0)^{1/2}$, although arguably not as accurately as in forced isotropic turbulence. In any case the most probable dynamic situation for an IVS inside the jet consists of an approximate balance between the opposing effects of viscous enstrophy diffusion and enstrophy production by axial stretching. For the IVSs near the jet edge, however, the absence of one fraction of the LVSs due to the proximity of the irrotational flow region, decreases the level of total axial stretching rate imposed on the IVSs, compared with the level of stretching found inside the jet. Owing to this, the radius of the IVSs near the jet edge will grow until they reach a new situation of equilibrium. Arguably, if an IVS is detrained and lost into the irrotational region, it will tend to grow even more due to the associated decrease of axial stretching as it moves farther away from the jet centreline. One must bear in mind, however, that since $T_\tau \ll T_U$ it is clear that the IVSs are dissipated in a very small time scale compared with the time associated with large-scale transport in the jet. Thus, it is highly unlikely that the IVSs from jets will be observed to decay as the jet evolves downstream.

Finally, note that in the present work no effort was made to separate the results depending on the local shape of the T/NT interface surface, i.e. whether the interface is convex or concave, such as is done in, e.g. Bisset *et al.* (2002), where it is shown that the conditional statistics in the convex outer part of the LVSs engulfing regions is different from the concave convoluted T/NT interface found near the centreline of the jet; however, this aspect certainly deserves to be investigated.

4.4. *Lifetime and characteristics of the intense vorticity structures inside the jet*

It is possible to make some rough estimates of the characteristics of the IVSs inside the shear layer, e.g. the vortex core radius, tangential velocity, vorticity and circulation, as the structures travel downstream in the jet. Before we do this, however, it is important to realize that the IVSs have a very small lifetime compared with the LVSs, and that for this reason it will be hard to visualize the scaling laws described here as

the IVSs travel downstream in a jet, since they will be quickly dissipated. Rather the relations derived here have to be understood as estimates for the existing IVSs at a particular downstream location in the jet. To see this we compare the lifetime of the IVSs with the characteristic time scale associated with their downstream transport in the jet. The time needed for an IVS to travel a distance equal to the integral scale L_{11} is $T_U = L_{11}/\bar{u}$, where $\bar{u}$ is the characteristic mean velocity in the jet, which is of the order of the centreline mean velocity $\bar{u} \sim \bar{u_0}$, while the integral scale inside the jet is roughly of the order of the jet half-width $L_{11} \sim \delta_{0.5}$ $(0.4 < L_{11}/\delta_{0.5} < 0.8)$ (Pope 2000). On the other hand, the lifetime of the IVS is of the order of the time corresponding to one rotation $T_\tau \sim R/u_0$. Given that the size of the vortex core radius is $R \sim \eta$, and using $u_0 \sim u'$, where u_0 is the maximum azimuthal velocity of the IVS, we have $T_\tau \sim \eta/u'$. In a planar jet $0.2 < u'/\bar{u_0} < 0.3$ for a range of Reynolds numbers $1500 < Re_H < 81\,400$ (Deo, Mi & Nathan 2008), therefore, by taking $u'/\bar{u_0} \approx 0.25$, we get $T_\tau/T_U \sim (R/u_0)(\bar{u_0}/L_{11}) \sim 4(\eta/L_{11}) \sim 4Re_0^{-3/4}$, where Re_0 is the Reynolds number of the large-scale eddies $Re_0 = u'L_{11}/\nu$. Clearly the lifetime of the IVS is much shorter than the time associated with their downstream transport.

The characteristics of the IVSs in a planar turbulent jet can be obtained using the theoretical results for the self-similar plane jet and considering that the IVSs are approximately described by the same scaling laws obtained by Jiménez & Wray (1998) in forced isotropic turbulence. The results described in the previous section support this view, e.g. in forced isotropic turbulence the radius of the IVS is of the order of the Burgers radius $R \sim R_B$ and as we have seen the same is also true in a jet, particularly deep inside the shear layer. Thus, the streamwise evolution of the vortex core size can be estimated assuming $R \sim R_B \sim (\nu/\sigma_0)^{1/2}$. Since the stretching rate is of the order of $\sigma_0 \sim \omega'$ and given that $\omega' \sim u'/\lambda$ (Jiménez & Wray 1998), and by using the relation for the downstream evolution of the Taylor micro-scale $\lambda \sim x^{3/4}$ (Antonia, Satyaprakash & Hussain 1980), one concludes that the IVS radius evolves as $R \sim x^{5/8}$. It is interesting to recall that in a plane jet the Kolmogorov micro-scale also evolves as $\sim x^{5/8}$ as shown by Deo *et al.* (2008) and Antonia *et al.* (1980), which shows that $R \sim \eta$ anywhere in the downstream evolution of the jet. Given that the Taylor-based Reynolds number increases in the jet as $Re_\lambda = u'\lambda/\nu \sim x^{1/4}$ (Antonia *et al.* 1980) it follows that the circulation evolves as $\Gamma \sim 20Re_\lambda^{1/2} \sim x^{1/8}$, and the axial vorticity as $\omega_0 \sim \omega' Re_\lambda^{1/2} \sim x^{-9/8}$. Finally, the maximum azimuthal velocity evolves as $u_0 \sim u' \sim x^{-1/2}$. Naturally we expect that as the T/NT interface is approached the IVS will tend to have a larger vortex radius, and smaller axial vorticity, circulation and azimuthal velocity than deep inside the shear layer for the reasons explained before. The present scaling laws for the IVSs could be assessed in a spatially evolving planar jet.

5. Conclusion

A DNS of a turbulent plane jet at $Re_\lambda = 120$ has been used to analyse the IVSs near the T/NT interface. The investigation used a tracking procedure to identify the IVSs which is similar (with some modifications) to the procedure developed by Jiménez *et al.* (1993) and Jiménez & Wray (1998). The T/NT interface is roughly defined by the radius of the LVSs at the edge of the jet, which is $R_{lvs} \sim \lambda$, while the IVSs appear more to the interior of the jet shear layer, at $\sim 5\eta$ from the location of the T/NT interface.

Well inside the jet shear layer the IVS characteristics are approximately similar to the IVSs observed in forced isotropic turbulence and several other flows: the mean

radius is of the order of the Kolmogorov micro-scale $\langle R\rangle/\eta = 4.6$, the tangential velocity is of the order of the root-mean-square velocity $\langle u_0\rangle/u' = 0.76$, the mean circulation Reynolds number normalized by the Taylor scale Reynolds number is $\langle Re_\Gamma\rangle/Re_\lambda^{1/2} \approx 28$ and the mean axial vorticity is $\langle \omega_0/(\omega' Re_\lambda^{1/2})\rangle = 0.38$, where ω' is the fluctuating vorticity norm. The shapes of the p.d.f.s of these quantities are also similar to the corresponding p.d.f.s in forced isotropic turbulence.

The mean size of the vortex core radius is also very close to the Burgers vortex radius $\langle R/R_B\rangle$ and the shape of the p.d.f.s of R/R_B are almost equal in the plane jet and in forced isotropic turbulence. This indicates that the IVSs from the jet are approximately described by the Burgers vortex model, i.e. for the IVSs inside a jet the enstrophy production by axial stretching is roughly balanced by the radial viscous diffusion indicating that the radius of the IVS is stable, as is the case in isotropic turbulence (Jiménez & Wray 1998).

The number of detected IVSs is roughly constant inside the jet but drops sharply in the region $5 < y_I/\eta < 20$. Virtually no IVSs exist in the region $0 < y_I/\eta < 5$ which can be explained by the size of the IVSs being approximately equal to $R/\eta \approx 5$ and therefore no IVSs can fit inside this thin layer.

Conditional statistics in relation to the distance from the T/NT interface were carried out in order to investigate how the IVS characteristics are affected by the presence of the T/NT interface. The radius, circulation, vorticity and tangential velocity are approximately constant inside the jet shear layer. When approaching the T/NT interface from the interior of the jet ($y_I/\eta \to 0$) the radius, circulation and tangential velocity increase near the jet edge, and display a maximum at about one Taylor micro-scale from the T/NT interface $y_I/\eta \approx 20$, before dropping again sharply in the region $5 < y_I/\eta < 20$. The axial vorticity is approximately constant across the shear layer.

The Burgers vortex is also a good model for the IVSs near the jet edge, although it is not as accurate as inside the jet shear layer. Indeed for the IVSs located at $5 < y_I/\eta < 20$, $\langle R/R_B\rangle \approx 0.90$. This is related with the level of axial stretching rate acting on the axis of the IVS σ_0, which is roughly constant inside the shear layer but decreases sharply near the T/NT interface attaining a minimum at $y_I/\eta \approx 20$. This is exactly the location where the radius, tangential velocity and circulation of the IVSs attain their maxima. The decrease in the magnitude of σ_0 near the jet edge can be explained by a decrease in the number of LVSs neighbouring the IVSs since the stretching imposed on the IVSs is known to originate in the background vorticity at the edges of the LVSs. Thus, the IVSs near the jet edge are not equilibrium Burgers vortices, and their mean radius will tend to increase in time. The lifetime of these structures, however, is small compared with the convective time scale making the temporal evolution of the radius hard to observe in a jet.

C.B.d.S. would like to acknowledge Professor J. Jiménez for interesting discussions on this theme during his visit to Madrid in March 2009 and during the visit of Professor J. Jiménez to Lisbon in November of the same year. Dr M. Teixeira is also acknowledged for interesting discussions on the topic of the T/NT interface. This work was supported by the Ministério da Ciência e da Tecnologia under grant number PTDC/EME-MFE/099636/2008.

Appendix. Vortex tracking algorithm

The vortex tracking algorithm implemented here is similar to Jiménez *et al.* (1993) with some modifications. The IVSs are defined as consisting of points where the vorticity $\omega = |\vec{\omega}|$ is above a certain threshold ω_{ivs}, where this threshold characterizes the points with the most intense vorticity existing within the flow domain. Following the procedure adopted by Jiménez *et al.* (1993), we define this threshold as equal to the vorticity of the points with highest enstrophy that are contained in 1 % of the total volume. In HIT the particular value used here was $\omega_{ivs} = 2.7\omega'$ and can be obtained from the histograms in figure 2. For comparison, Jiménez *et al.* (1993) obtained $\omega_{ivs} = 3.1\omega'$ at similar Reynolds number.

As a pre-processing step in the tracking algorithm all of the identified points, i.e. points with vorticity above the defined threshold $\omega > \omega_{ivs}$ are listed and ordered. Each axis is then identified according to the following steps: (i) choose the first non-assigned point; (ii) choose the nearest grid plane intersected by the direction of $\vec{\boldsymbol{\omega}}$; the four points in this plane which are nearest to the intersection are chosen as candidates; (iii) choose the point with the highest value of ω that has not yet been assigned. The algorithm stops when all points have been assigned. In a second post-processing phase all IVS points belonging to an axis with less than 20 points are discarded. A modification introduced here that is absent from the tracking described in Jiménez *et al.* (1993) is the elimination of all clustered axis points (i.e. points from two parallel axis), leaving only points from the axis with the strongest enstrophy.

The worm radius and circulation as function of axis position are calculated from the vorticity profile along the axis. This profile is obtained using the following steps: (i) a plane normal to the direction of the vorticity vector is defined for each identified point; (ii) the vorticity $\vec{\omega}$ can be interpolated into any given point on this plane using the least-squares method; in the present work $n = 6$ radial bins centred on the axis, with a radius equal to $n\Delta x$, and with $m = 8$ points per bin, with an angular interval equal to $2\pi/m$ were used; (iii) to compensate for the noise induced by the discretization, the value obtained for the radial distribution is filtered over triples of consecutive axial locations using a [1/4, 1/2, 1/4] mask.

The worm radius R is calculated by an iterative fit of the axial distribution to $\omega = \omega_0 \mathrm{e}^{-r^2/R^2}$, where ω_0 is the value of vorticity at the axis point. All points where the iterative process was unable to converge were discarded, like those with a very large radius $R > 30\eta$, as in Jiménez & Wray (1998).

The tangential (or azimuthal) velocity was computed using two different methods. The first method assumes a Gaussian distribution for the vorticity in each IVS $\omega(r) = \omega_0 \mathrm{e}^{-r^2/R^2}$. Using the relation $\oint \vec{u}\,\mathrm{d}\vec{l} = \int\int \vec{\omega}\vec{n}\,\mathrm{d}S$ with the assumed vorticity distribution one obtains the expression for the tangential velocity $u_0 = 0.316\omega_0 R$.

In the second method the tangential velocity is determined directly from the velocity flow field. A plane normal to the ω_0 axis is determined and the flow field vectors are projected into it. The tangential velocity is then obtained at each radial position using an azimuthal averaging procedure similar to that described above. The two methods give similar results for u_0. In the present work the second method was used since it requires no assumption on the shape of the vorticity distribution.

REFERENCES

ANAND, R. K., BOERSMA, B. J. & AGRAWAL, A. 2009 Detection of turbulent/non-turbulent interface for an axisymmetric turbulent jet: evaluation of known criteria and proposal of a new criterion. *Exp. Fluids* **47** (6), 995–1007.

ANTONIA, R. A., SATYAPRAKASH, B. R. & HUSSAIN, A. K. M. F. 1980 Measurements of dissipation rate and some other characteristics of turbulent plane and circular jets. *Phys. Fluids* **23** (4), 695–700.

ASHUST, W., KERSTEIN, A., KERR, R. & GIBSON, C. 1987 Alignment of vorticity and scalar gradient with strain rate in simulated Navier–Stokes turbulence. *Phys. Fluids* **30**, 2343.

BISSET, D. K., HUNT, J. C. R. & ROGERS, M. M. 2002 The turbulent/non-turbulent interface bounding a far wake. *J. Fluid Mech.* **451**, 383–410.

CORRSIN, S. & KISTLER, A. L. 1955 Free-stream boundaries of turbulent flows. NACA Tech Rep. TN-1244.

DAVIDSON, P. A. 2004 *Turbulence, an Introduction for Scientists and Engineers*. Oxford University Press.

DEO, R. C., MI, J. & NATHAN, G. J. 2008 The influence of Reynolds number on a plane jet. *Phys. Fluids* **20**, 075108.

DUBIEF, I. & DELCAYRE, F. 2000 On coherent-vortex identification in turbulence. *J. Turbul.* **1** (011).

GANAPATHISUBRAMANI, B., LAKSHMINARASIMHAN, K. & CLEMENS, N. T. 2008 Investigation of three-dimensional structure of fine scales in a turbulent jet by using cinematographic stereoscopic particle image velocimetry. *J. Fluid Mech.* **598**, 141–175.

HOLZNER, M., LIBERZON, A., NIKITIN, N., KINZELBACH, W. & TSINOBER, A. 2007 Small-scale aspects of flows in proximity of the turbulent/non-turbulent interface. *Phys. Fluids* **19**, 071702.

HUNT, J. C. R., EAMES, I. & WESTERWEEL, J. 2008 Vortical interactions with interfacial shear layers. In *Proceedings of IUTAM Conference on Computational Physics and New Perspectives in Turbulence, Nagoya, September 2006* (ed. Y. Kaneda). Springer Science.

HUNT, J. C. R., EAMES, I., WESTERWEEL, J., DAVIDSON, P. A., VOROPAYEV, S., FERNANDO, J. & BRAZA, M. 2010 Thin shear layers – the key to turbulence structure. *J. Hydro-Environment Research* **4**, 75–82.

JIMÉNEZ, J. & WRAY, A. 1998 On the characteristics of vortex filaments in isotropic turbulence. *J. Fluid Mech.* **373**, 255–285.

JIMÉNEZ, J., WRAY, A., SAFFMAN, P. & ROGALLO, R. 1993 The structure of intense vorticity in isotropic turbulence. *J. Fluid Mech.* **255**, 65–90.

KANG, S.-J., TANAHASHI, M. & MIYAUCHI, T. 2008 Dynamics of fine scale eddy clusters in turbulent channel flows. *J. Turbul.* **8** (52), 1–19.

KIDA, S. & MIURA, H. 1998 Identification and analysis of vortical structures. *Eur. J. Mech.* (B/*Fluids*) **17** (4), 471–489.

LESIEUR, M. 1997 *Turbulence in Fluids*, 3rd edn. Kluwer.

MATHEW, J. & BASU, A. 2002 Some characteristics of entrainment at a cylindrical turbulent boundary. *Phys. Fluids* **14** (7), 2065–2072.

MOURI, H., HOURI, A. & KAWASHIMA, Y. 2007 Laboratory experiments for intense vortical structures in turbulence velocity fields. *Phys. Fluids* **19**, 055101.

POPE, S. B. 2000 *Turbulent Flows*. Cambridge University Press.

SIGGIA, E. D. 1981 Numerical study of small-scale intermittency in three-dimensional turbulence. *J. Fluid Mech.* **107**, 375–406.

DA SILVA, C. B. 2009 The behavior of subgrid-scale models near the turbulent/nonturbulent interface in jets. *Phys. Fluids* **21**, 081702.

DA SILVA, C. B. & PEREIRA, J. C. F. 2007*a* Analysis of the gradient-diffusion hypothesis in large-eddy simulations based on transport equations. *Phys. Fluids* **19**, 035106.

DA SILVA, C. B. & PEREIRA, J. C. F. 2007*b* Enstrophy, strain and scalar gradient dynamics across the turbulent–nonturbulent interface in jets. In *Advances in Turbulence XI – 11th Euromech ETC, Porto*.

DA SILVA, C. B. & PEREIRA, J. C. F. 2008 Invariants of the velocity-gradient, rate-of-strain, and rate-of-rotation tensors across the turbulent/nonturbulent interface in jets. *Phys. Fluids* **20**, 055101.

DA SILVA, C. B. & PEREIRA, J. C. F. 2009 Erratum: 'invariants of the velocity-gradient, rate-of-strain, and rate-of-rotation tensors across the turbulent/nonturbulent interface in jets' [*Phys. Fluids* **20**, 055101 (2008)]. *Phys. Fluids* **21**, 019902.

DA SILVA, C. B. & DOS REIS, R. N. 2011 The role of coherent vortices near the turbulent/nonturbulent interface in a planar jet. *Phil. Trans. R. Soc.* A **369**, 738–753.

DA SILVA, C. B. & TAVEIRA, R. R. 2010 The thickness of the turbulent/nonturbulent interface is equal to the radius of the large vorticity structures near the edge of the shear layer. *Phys. Fluids* **22**, 121702.

STANLEY, S., SARKAR, S. & MELLADO, J. P. 2002 A study of the flowfield evolution and mixing in a planar turbulent jet using direct numerical simulation. *J. Fluid Mech.* **450**, 377–407.

TANAHASHI, M., IWASE, S. & MIYAUCHI, T. 2001 Appearance and alignment with strain rate of coherent fine scale eddies in turbulent mixing layer. *J. Turbul.* **2** (6), 1–17.

TOWNSEND, A. A. 1966 The mechanism of entrainment in free turbulent flows. *J. Fluid Mech.* **26**, 689–715.

TOWNSEND, A. A. 1976 *The Structure of Turbulent Shear Flow*. Cambridge University Press.

VINCENT, A. & MENEGUZZI, M. 1991 The spatial structure and statistical properties of homogeneous turbulence. *J. Fluid Mech.* **225**, 1–20.

WESTERWEEL, J., FUKUSHIMA, C., PEDERSEN, J. M. & HUNT, J. C. R. 2005 Mechanics of the turbulent-nonturbulent interface of a jet. *Phys. Rev. Lett.* **95**, 174501.

WESTERWEEL, J., FUKUSHIMA, C., PEDERSEN, J. M. & HUNT, J. C. R. 2009 Momentum and scalar transport at the turbulent/non-turbulent interface of a jet. *J. Fluid Mech.* **631**, 199–230.